

The Inhibition Effect and Mechanism of 4H-1,2,4-triazol-3-amine and Three Schiff Bases Self-Assembled Films on the Corrosion of Carbon Steel

Zhe Zhang¹, Le Ruan^{1,*}, Xiaodong Huang¹, Yuzeng Lyu², Shuhua Zhang¹, Wei Shang¹, Xiuying Li¹, Ling Wu³

¹ Guangxi Key Laboratory of Electrochemical and Magneto-chemical Functional Materials, College of Chemistry and Bioengineering, Guilin University of Technology, Guilin 541004, PR China

² Engineering Research Center of Exploration for hidden Nonferrous and Precious Metal Ore Deposits, Ministry of Education, Guilin 541004, PR China

³ School of Chemistry and Chemical Engineering, Shandong University, Jinan 250100, PR China

*E-mail: ruanle@glut.edu.cn

Received: 6 July 2016 / Accepted: 4 November 2016 / Published: 12 December 2016

4H-1,2,4-triazol-3-amine and its aldehyde Schiff bases self-assembled films were formed on carbon steel surface. Electrochemical impedance spectroscopy and polarization curve measurements showed that the self-assembled films could protect carbon steel from corrosion in 0.5M HCl solution. X-ray photoelectron spectroscopy (XPS) analyses indicated that the chemisorption of triazol-3-ylamine and three Schiff bases molecules on carbon steel surface through N atom and ring. Quantum chemical calculation and dynamic simulation were used to further investigate the inhibition mechanism.

Keywords: Schiff base; self-assembled films; carbon steel; EIS; XPS.

1. INTRODUCTION

Carbon steels are widely used in industry as the basic materials for modern materials science and engineering [1, 2]. The corrosion of steel brings inestimable damage to the human life and production, so slowing down or completely inhibiting corrosion has been an intensive field of interest [3]. Self-assembly Technology is a useful method to deal with this problem by forming self-assembled (SA) films on metal surface which can prevent the metal contacting the erosive solution [4-6]. Compounds that contain heteroatoms with a lone pair of electrons such as N, O, S and P atoms and multiple bonds or aromatic rings are the most efficient self-assembled molecules since a bond can be formed between the electron pair and/or the electron cloud of the donor atoms and the metal surface, thereby reducing corrosive attack in acidic media [7-9].

Acid solution are often used in industry for cleaning, descaling and pickling of metallic structures, which are accompanied by dissolution of the metal [10]. It has been previously reported that the inhibition efficiency of carbon steel can be significantly improved by modifying the surface with SA films in acid solutions [11, 12].

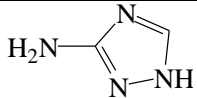
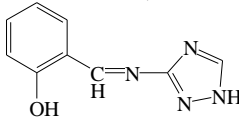
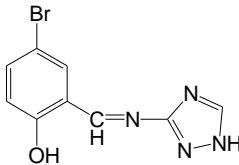
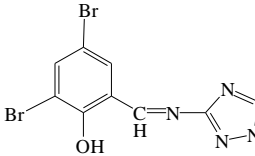
Due to the presence of C=N groups, Schiff bases have excellent corrosion inhibition ability. The planarity of p electrons and pair of electrons on the N atoms are the important structural features of C=N groups that lead to the adsorption of these molecules to the metal surface [13, 14]. Negm et al [15] studied the inhibition effect of two synthesized quaternary isoxazolium Schiff bases on carbon steel in HCl solution using gravimetric and electrochemical measurements. Results showed a gradual increase in the inhibition efficiency by increasing the hydrophobic chain length. Three Schiff bases were synthesized and investigated as corrosion inhibitors for mild steel by Ansari et al, and the highest inhibition efficiency of (3-phenylallylidene) amino-5-(pyridine-4-yl)- 4H-1,2,4-triazole-3-thiol was 96.6% [16].

In this work, electrochemical impedance spectroscopy (EIS) and polarization curves were used to investigate the corrosion effect of 4H-1,2,4-triazol-3-amine (TA), N-[(3'-Hydroxyphenyl)methylidene]-4H-1,2,4-triaamine (HMTA), 4-Bromo-2-[(E)-(1H-1,2,4-triazol-3-ylimino)-methyl]-phenol (BHMTA) and N-[(3', 5'-Dibromo-2'-hydroxyphenyl)methylidene] 1,2,4-triazol-3-amine (DHMTA) SA films on carbon steel surfaces. Schiff base SA films were characterized by X-ray photoelectron spectroscopy (XPS), quantum chemical calculations and molecular dynamic approach were used to study the binding properties of compounds on carbon steel surfaces.

2. EXPERIMENTAL

2.1. Materials

Table 1. The chemical structures and abbreviations of 4H-1,2,4-Triazol-3-Amine and three Schiff bases

Chemical	Structure	Abbreviation
4H-1,2,4-Triazol-3-Amine		TA
N-[(3'-Hydroxyphenyl)methylidene]-4H-1,2,4-triaamine		HMTA
4-Bromo-2-[(E)-(1H-1,2,4-triazol-3-ylimino)-methyl]-phenol		BHMTA
N-[(3', 5'-Dibromo-2'-hydroxyphenyl)methylidene] 1,2,4-triazol-3-amine		DHMTA

A 4.0mm diameter low carbon steel rod with a composition: element (wt. %) C (0.22), Si (0.35), Mn (1.4), S (0.05), P (0.045) and Fe (balance) was used in this study, sanded using 500[#], 1000[#] and 1400[#] emery papers, respectively. After the surface polished, the carbon steel electrode was cleaned with ethanol using an ultrasonic cleaner.

The 0.5M HCl solution was used as the corrosion medium, which was prepared from analytical-grade HCl (12M) and ultrapure water. All the chemical reagents and TA were purchased from Aladdin Industrial Corporation. 4H-1,2,4-triazol-3-amine, salicylaldehyde, and 2-Bromosalicylaldehyde were used to synthesis the three kinds of Schiff base compounds [17-19]. The chemical structures and abbreviations of three Schiff base compounds are shown in Table 1.

2.2. Preparation of SA films

TA and three Schiff base compounds were dissolved in ethanol to produce the 0.005 M self-assembly solution. The cleaned carbon steel electrodes were immersed in the different self-assembly solution for 0 h, 2 h, 4 h, 6 h, 8 h and 10 h at a room temperature of 25 °C.

2.3. Electrochemical measurements

The working cell was a traditional three-electrode cell having the carbon steel specimen as the working electrode, two Pt sheets as counter electrode and a saturated calomel electrode (SCE) as the reference electrode. EIS and polarization curves were carried out on an electrochemical workstation (CHI 760, China) with the samples immersed in 0.5 M HCl. EIS tests were carried out at the open circuit potential using a 5 mV amplitude sinusoidal signal over the frequencies ranging from 100 kHz to 0.1 Hz. The potential in polarization curve measurement increased with a rate of 2 mV s⁻¹ started from -200 to +200 mV with respect to the open circuit potential versus corrosion potential.

2.4 XPS measurements

Samples for XPS experiments were carbon steel sheets (3 mm × 3 mm × 1 mm), and the preliminary process was the same as above. The carbon steel specimen was immersed in the 0.005 M DHMTA solution for 10 h, then rinsed with ultrapure water and dried for testing. The XPS spectra were taken by ESCALAB 250 Xi system (Thermo Electron Corporation, USA). The excitation source was Al K α radiation (photoelectron energy of 1253.6 eV). Survey scans and relevant core levels were recorded: Cu 2p_{1/2}, Br 2p_{3/2}, N 1s, C 1s and O 1s. The XPS data were fitted with XPS peak41 software.

2.5. Quantum chemical study and molecular dynamic simulation

Quantum chemical study were performed with Gaussian 03 W software package, using B3LYP model of density functional theory (DFT) with 6-311G* basis sets [20, 21]. The geometry of Schiff

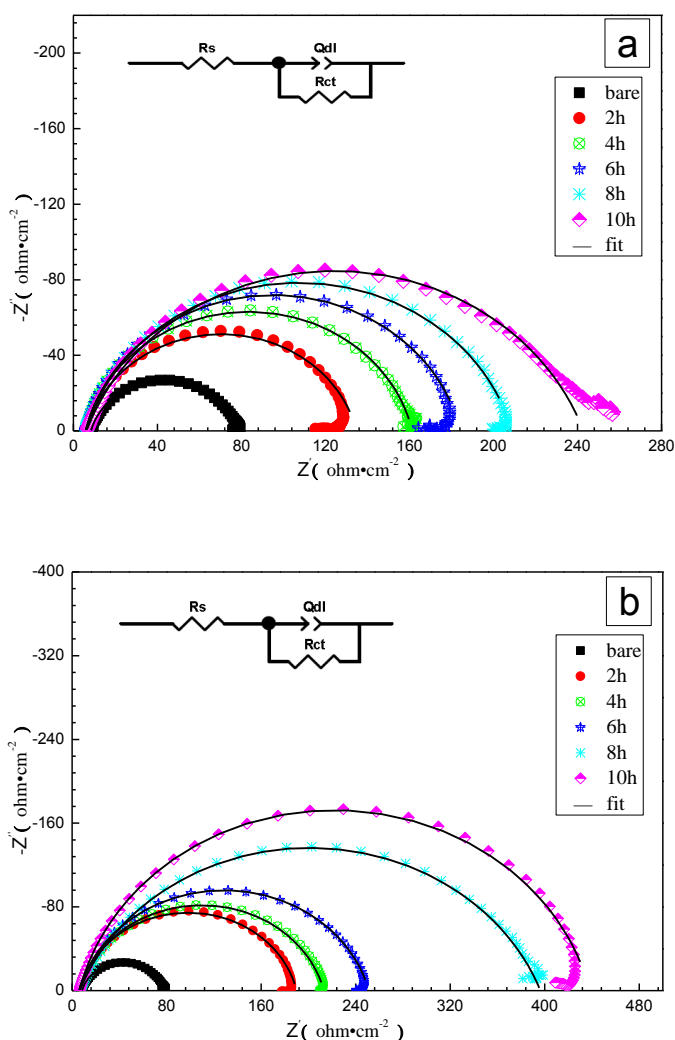
bases molecular system was optimized and the highest occupied molecular orbital energy (E_{HOMO}), the lowest unoccupied molecular orbital energy (E_{LUMO}) and electron density distribution were calculated to evaluate the effect on the inhibition abilities.

Molecular dynamic simulations were performed using the Discover module of the Materials Studio 6.0 software [22]. The simulated solution system was 0.5 M HCl solution containing 400 H_2O , 4 H_3O^+ , 4 Cl^- and 1 SA molecule. The model metal surface comprised of a Fe crystal cleaved along the (1 1 0) plane, with a vacuum layer on the topside [23].

Build/Symmetry/Supercell method was used to build the super cell. The solution system was added on the surface of Fe crystal and the geometry of the system was optimized so that the energy of the system was at a local minimum with respect to potential energy. The canonical ensemble NVT was performed at 298.0 K and the simulation time was 500 ps with a time step of 1.0 fs using the COMPASS force field.

3. RESULT AND DISCUSSION

3.1. EIS measurement



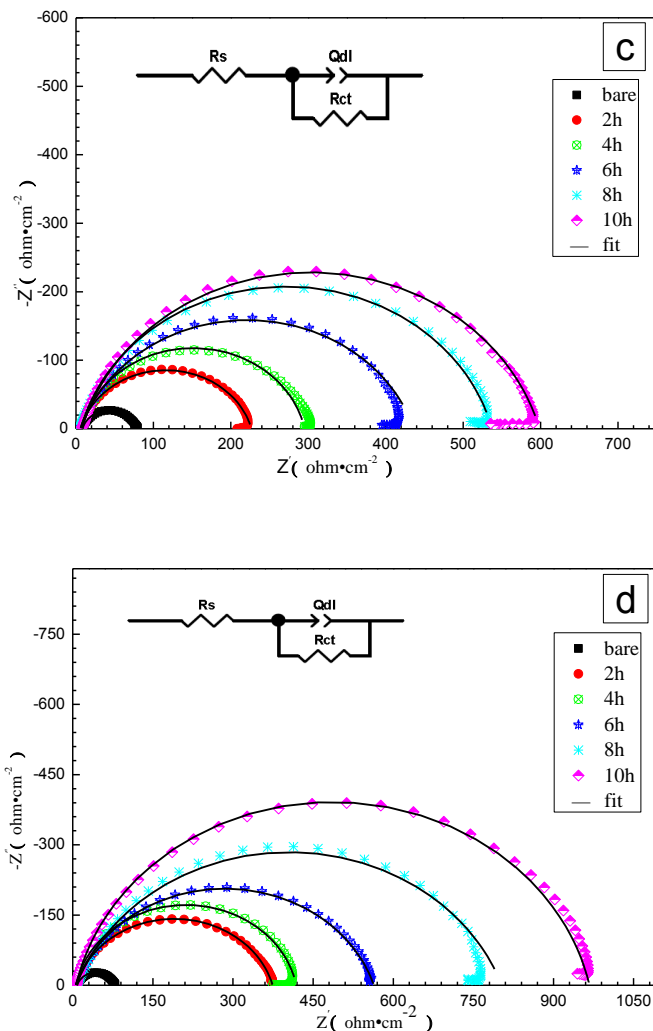


Figure 1. Nyquist impedance spectra of the carbon steel electrode covered with and without SAfilms in 0.5 M HCl solutions with a long immersion time in TA (a), HMTA (b), BHMTA(c) and DHMTA (d) solutions. The solid lines are their fitted curves

Fig. 1 represents the electrochemical impedance spectra obtained on the carbon steel modified without and with TA, HMTA, BHMTA and DHMTA SA films at different immersion time. It is clearly seen that the carbon steel electrodes covered with TA and Schiff bases SA films show depressed semicircles whose diameters get larger with the increase of immersion time from 2 h to 10 h. This indicates that the increase of the immersion time decrease the dissolution of steel in HCl solution through increasing its corrosion resistance. All impedancespectra for Nyquist plots are analyzed by fitting to the equivalent circuitshown in Fig. 1. The parameters of the used circuit can be defined as follows: R_s represents the solution resistance, R_{ct} represents the charge transfer resistance, Q_{dl} is the constant phase elements (CPE) defined by the value of Y_0 and n :

$$Y_{CPE} = Y_0(j\omega)^{-n} \tag{1}$$

$$Z_{CPE} = \frac{I}{Y_0} (j\omega)^n \tag{2}$$

where Y_0 is modulus, j is the imaginary root, ω is the angular frequency and n is the phase.

Table 2. Element value of a circuit equivalent to fit the impedance spectra in Figure 1 and the values of the protection efficiency (η) calculated by Eq. (3).

Assembly mo molecule	Immersion Time (h)	R_s (Ωcm^2)	R_{ct} (Ωcm^2)	CPE		C_{dl} ($\mu\text{F cm}^{-2}$)	η (%)
				n (0-1)	Y_0 ($\mu\Omega^{-1}\text{s}^n\text{cm}^{-2}$)		
bare	0	8.32	69.94	0.84	44.26	14.226	—
	2	6.18	128.3	0.86	22.00	8.269	45.49
	4	5.81	155.6	0.87	20.13	8.335	55.05
TA	6	5.94	178.2	0.86	20.79	8.611	60.75
	8	5.96	200.7	0.84	19.25	6.684	65.15
	10	6.24	236.5	0.79	20.07	4.875	70.43
HMTA	2	6.31	184	0.87	17.26	7.144	61.99
	4	6.02	207.1	0.85	17.97	6.668	66.23
	6	5.97	244.7	0.85	16.95	6.210	71.42
BHMTA	8	5.96	386.9	0.82	21.26	7.511	81.92
	10	6.16	432.4	0.86	12.07	5.037	83.83
	2	5.93	220.6	0.84	18.12	6.287	68.30
DHMTA	4	7.43	289.9	0.87	10.25	4.373	75.87
	6	6.01	428.8	0.81	13.81	4.140	83.69
	8	5.82	530.5	0.84	13.57	5.484	86.82
DHMTA	10	7.70	589.8	0.84	8.72	3.148	88.14
	2	6.18	368.1	0.84	14.98	5.431	81.00
	4	6.13	411.2	0.88	12.53	6.286	82.99
DHMTA	6	5.76	557.9	0.81	15.12	4.964	87.46
	8	6.57	789.9	0.79	7.50	1.926	91.15
	10	6.26	961	0.87	9.43	4.685	92.72

The inhibition efficiency obtained from the charge transfer resistance is calculated with Eq. 3:

$$\eta_R = \frac{R_{ct} - R_{ct}^0}{R_{ct}} \times 100\% \quad (3)$$

where R_{ct} and R_{ct}^0 are the charge transfer resistance values with and without SA films on carbon steel surface, respectively. The values of CPE capacitance (C_{dl}) are calculated using Eq. (4) [24]:

$$C_{dl} = \frac{\epsilon_0 \epsilon}{d} S \quad (4)$$

where ϵ_0 is the permittivity of air, ϵ is the local dielectric constant, d is the film thickness and S is the electrode surface. All the data are collected in Table 1. It can be seen that the C_{dl} values decrease with the immersion time prolonging, which is attributed to the replacement of the adsorbed H_2O molecules at the carbon steel surface by the inhibitor molecule having a lower dielectric constant [25]. The inhibition efficiency of the SA films on carbon steel surface increases with the immersion time and after immersing in the assembling solution for 10 h, the inhibition efficiencies of the electrodes covered with TA, HMTA, BHMTA and DHMTA SA films reach 70.43%, 83.83%, 88.14% and 92.72%, respectively. All the inhibitor molecules contain triazole rings which can be adsorbed on the carbon steel surface by providing π -electrons to form SA films. The benzene ring and $-RC=N-$ groups in HMTA, BHMTA and DHMTA molecules facilitate the absorbance of these groups on the carbon steel surface. The halogen functional groups of Br- also can increase the ability of accepting electrons, so the corrosion efficiency of the SA films follows the order: TA < HMTA < BHMTA < DHMTA. The fact that R_{ct} and the inhibition efficiency increase with assembling time indicates considerable surface coverage by the Schiff base compounds and strong bonding to the surface [26].

3.2. Polarization curve investigation

The polarization curves for carbon steel electrodes covered with SA films at various immersion times are presented in Fig. 2 and all the polarization parameters are listed in Table 3. The corrosion efficiency (η) is calculated using the following equation:

$$\eta = \frac{i_{corr}^0 - i_{corr}}{i_{corr}^0} \times 100\% \quad (5)$$

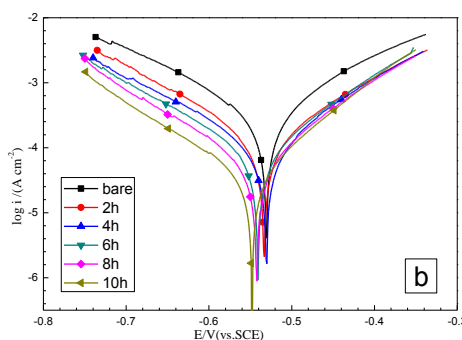
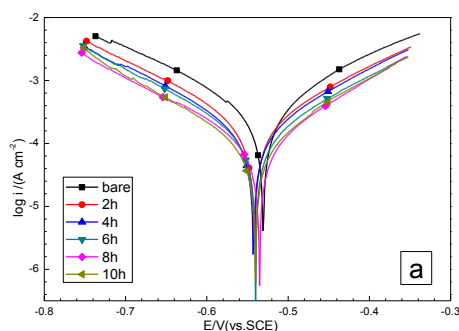
where i_{corr}^0 and i_{corr} represent the corrosion densities of the bare and SA film modified carbon steel electrodes, respectively.

As it can be seen from Fig. 2, the Tafel slopes decrease to more negative potential and increase to more positive potentials relative to the bare electrode curve, which indicates that the anodic and cathodic reaction of the electrodes are suppressed after modified with SA films. The E_{corr} values of the electrodes change slightly after covering with TA and Schiff bases SA films, so all the TA and Schiff bases are mix-type inhibitor by inhibiting both hydrogen evolution and carbon steel dissolution reaction [27]. The i_{corr} values of the electrodes modified with SA films decrease with the immersion time. The η of the SA films formed by immersing in the TA, HMTA, BHMTA and DHMTA solution for 10 h are 69.21%, 82.32%, 87.15% and 95.35% respectively, which is consistent with the observations from the EIS measurements. The inhibition efficiency is affected by the number of adsorption sites, molecular size and mode of interaction with the metal surface [28]. The π -electrons in

the molecule has an very important role on the adsorption, all the three Schiff base compounds have benzene ring and triazol ring, so they can form self-assembled film on carbon steel surface and protect it from corrosion[29].

Table 3. Polarization parameters for the bareworking electrode and working electrodes covered with various SA films in 0.5 M HCl solution

Assembly molecules	Immersion time (h)	E_{corr} (V vs .SCE)	$-\beta_a$ (V dec ⁻¹)	β_c (V dec ⁻¹)	i_{corr} (μ Acm ⁻²)	η (%)
bare	0	-0.5314	0.149	0.129	310.4	—
	2	-0.542	0.137	0.137	188.2	39.37
	4	-0.542	0.136	0.131	155.2	50.00
TA	6	-0.541	0.135	0.132	132.4	57.35
	8	-0.536	0.159	0.128	109.8	64.63
	10	-0.541	0.134	0.119	95.56	69.21
HMTA	2	-0.534	0.137	0.130	129	58.44
	4	-0.53	0.145	0.116	100	67.78
	6	-0.542	0.135	0.111	85.9	72.33
BHMTA	8	-0.542	0.137	0.107	58.03	81.30
	10	-0.543	0.135	0.090	54.88	82.32
	2	-0.543	0.144	0.102	99.26	68.02
DHMTA	4	-0.546	0.146	0.104	88.53	71.48
	6	-0.549	0.134	0.090	50.26	83.81
	8	-0.529	0.138	0.086	44.86	85.55
DHMTA	10	-0.547	0.148	0.095	39.9	87.15
	2	-0.535	0.133	0.097	75.61	75.64
	4	-0.529	0.132	0.099	51.07	83.55
DHMTA	6	-0.528	0.132	0.099	51.07	83.55
	8	-0.536	0.130	0.093	37.09	88.05
	10	-0.532	0.115	0.082	14.43	95.35



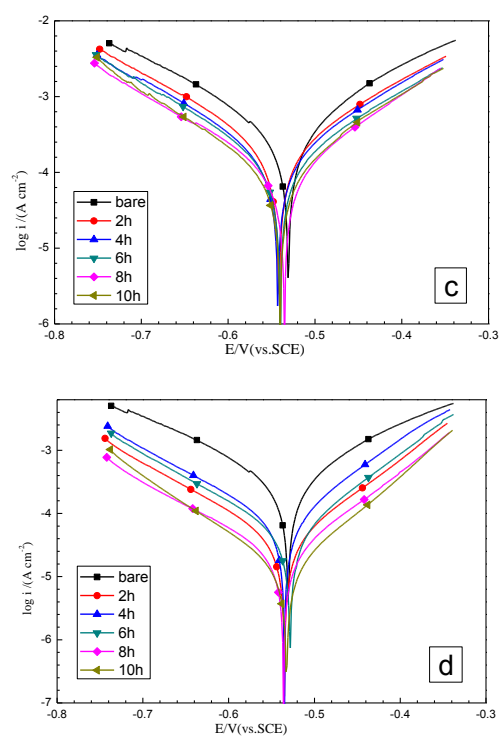


Figure 2. Polarization curves of the bare working electrode and the working electrodes covered with SA films measured in a 0.5 M HCl solution with prolonged immersion time in 0.005 M TA(a), 0.005M HMTA(b), 0.005 M BHMTA(c) and 0.005 DHMTA(d) solutions.

3.3. XPS studies

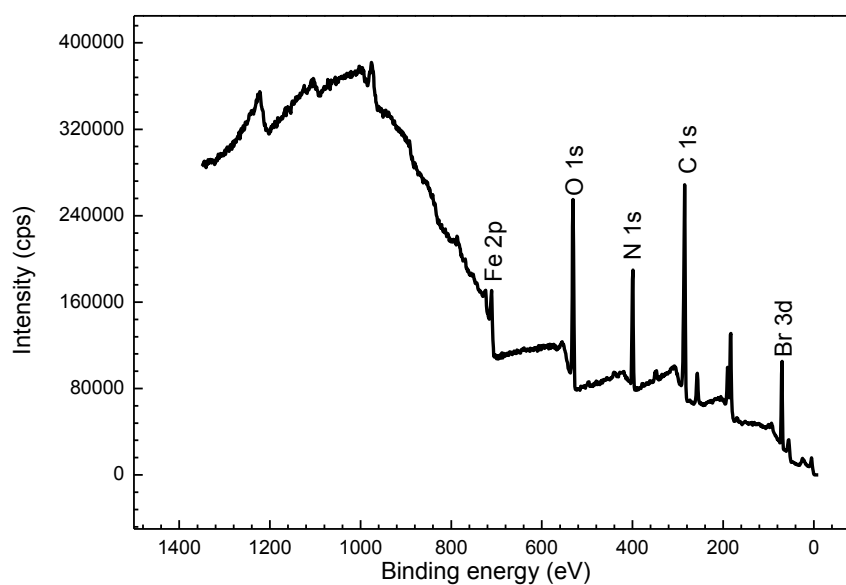


Figure 3. Wide-scan XPS spectrum of the carbon steel surfacemodified with DHMTA SA films.

To further investigate the surface composition of DHMTA SA films on carbon steel, XPS analysis was performed. The wide-scan XPS spectrum is shown in Fig. 3. The corrosive carbon steel shows the XPS spectra of Fe 2p, O 1s, N 1s, C 1s and Br 3d, which confirms the presence of the DHMTA films on the modified carbon steel surface.

The high-resolution XPS spectra of Fe 2p, O 1s, N 1s, C 1s and Br 3d are shown in Fig. 4. All the peaks are fitted to confirm the component by checking the elements of the energy of XPS [30].

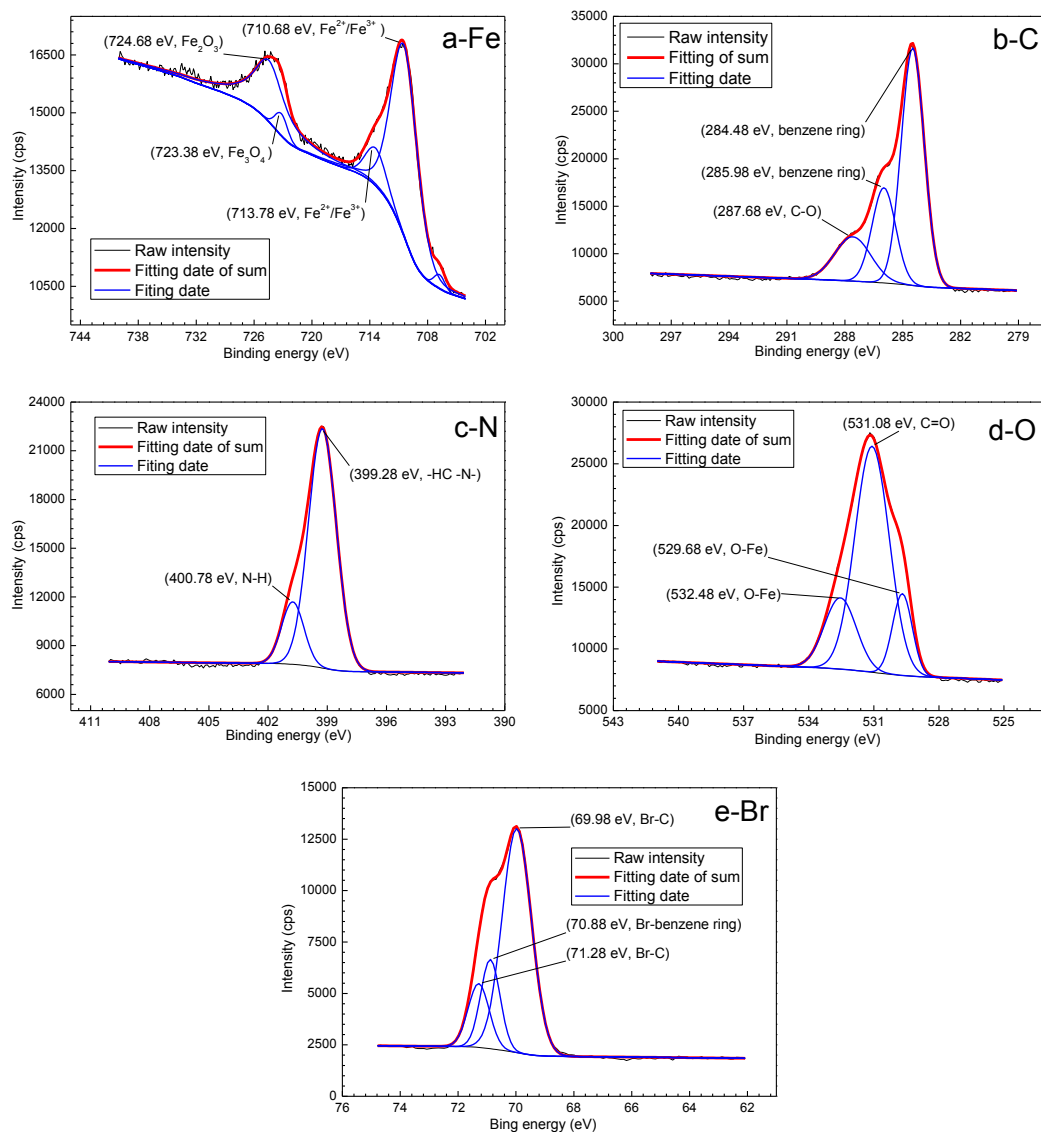


Figure 4. High-resolution XPS spectra of DTYMP self-assembling films: (a) Fe2p, (b) C1s, (c) N1s, (d) O1s, (e) Br3d.

Fig. 4 shows the peaks for Fe 2p at 710.68 eV, 713.78 eV, 723.38 eV and 724.68 eV. The composition of 710.68 eV and 713.78 eV is $\text{Fe}^{2+}/\text{Fe}^{3+}$ and the peak of 723.38 eV and 724.68 eV are Fe_3O_4 and Fe_2O_3 , respectively, which is due to the oxidation of Fe during the preparation process of SA films. The peaks at 284.48 eV and 285.98 eV in Fig. 4b is attributable to the benzene rings of DHMTA molecules. The peak at 287.68 eV is attributable to the absorption peak of C-O group. The N

2s spectrum (Fig. 4c) for DHMTA SA films shows two peaks at 399.28 eV and 400.78 eV caused by -CH-N- and N-H groups. The O 1s spectrum (Fig. 4d) can be decomposed into 3 peaks. The first peak around 531.08 eV is attributed to C-O, 529.68 eV and 532.48 eV are attributed to some iron oxides. The peaks of 69.98 eV, 70.88 eV and 71.28 eV in Fig 4e indicate the Br atoms from the SA molecule combination with carbon steel. Therefore, the XPS measurements indicate that DHMTA molecules can adsorb on the carbon steel surface and form SA film to prevent it from corrosion.

3.4. Quantum chemical calculations

Fig. 5 shows the HOMO density distribution and the LUMO density distribution with DFT at the B3LYP/6-311* level of theory. A high E_{HOMO} value expresses intrinsic electron donating tendency to an appropriate acceptor and the E_{LUMO} signifies the electron receiving tendency of a molecule. It can be seen the HOMO of TA is distributed over benzotriazole and amino groups, the HOMO of HMTA, BHMTA and DHMTA is distributed mainly over benzotriazole, -C-N-, benzene ring and -C-Br groups. The LUMO of TA is distributed all over the molecule and the LUMO of the three Schiff bases is distributed over the inhibitor molecule except for hydrogen atoms. It can be concluded the unoccupied d orbit of Fe can both form coordinate bond with HOMO orbit and form back-donation bond with LUMO orbit. So the Schiff base molecules are in combination with carbon steel surface with chemical bond which prevent the carbon steel from corrosion in the erosive solution.

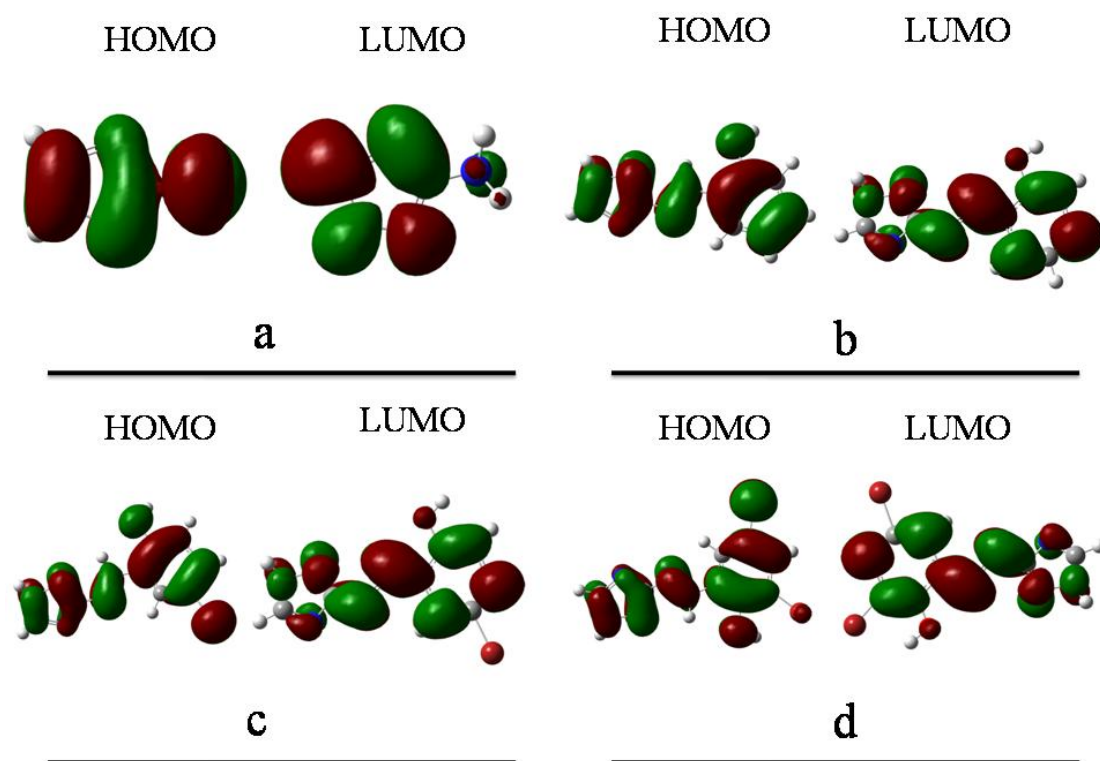


Figure 5. The HOMO and LUMO molecular orbitals of inhibitors molecule: TA(a), HMTA(b), BHMTA(c), DHMTA(d).

The calculated quantum chemical indices E_{HOMO} , E_{LUMO} , energy gap ΔE ($\Delta E = E_{\text{LUMO}} - E_{\text{HOMO}}$) and dipole moment (μ) are given in Table 4. The energies of E_{HOMO} and E_{LUMO} are related to the ionization potential (I) and the electron affinity (A) of the iron atoms and the inhibitor molecules, defined as $I = -E_{\text{HOMO}}$ and $A = -E_{\text{LUMO}}$. The absolute electronegativity (χ) and the global hardness (γ) of the inhibitor molecule are approximated by Eqs. (6) and (7):

$$\chi = \frac{I + A}{2} \quad (6)$$

$$\gamma = \frac{I - A}{2} \quad (7)$$

Thus, the fraction of electrons transferred from the inhibitor to metallic surface (ΔN) is calculated by Eq. (8) [31]:

$$\Delta N = \frac{\chi_{\text{Fe}} - \chi_{\text{inh}}}{2(\gamma_{\text{Fe}} + \gamma_{\text{inh}})} \quad (8)$$

where the χ_{Fe} and γ_{Fe} are the absolute electronegativity and global hardness of the Fe atom, and the χ_{inh} and γ_{inh} are the absolute electronegativity and global hardness of the self-assembled molecules. The theoretical values of χ_{Fe} and γ_{Fe} are 7 eV and 0 eV [32]. According to Lukovits, if $\Delta N < 3.6$, the inhibition efficiency increases with increasing electron-donating ability at the metal surface [33]. The ΔN values for TA and other three Schiff bases are all less than 3.6, which means that the increase in inhibition efficiency is due solely to the electron donating ability of the inhibitor. From the results obtained from frontier molecular orbitals and frontier orbital energies, it can be concluded that the DHMTA has the highest capabilities to accept electrons from the metal surface according to Saha et al [34].

Table 4. Quantum chemical parameters calculated using the B3LYP method with a 6-311G (d, p) basis set for and inhibitors molecules

Molecule molecule	E_{HOMO} (eV)	E_{LUMO} (e V)	ΔE (eV)	μ (Debye)	$\chi = (I+A) / 2$	$\gamma = (I-A)/2$	ΔN	η_{10h} (%)
TA	-5.98	0.23	6.21	2.00	2.88	3.10	1.33	70.43
HMTA	-6.10	-1.68	4.43	3.27	3.89	2.21	1.41	83.83
BHMTA	-6.23	-1.94	4.29	5.12	4.08	2.14	1.36	88.14
DHMTA	-6.43	-2.15	4.28	4.27	4.29	2.14	1.27	92.72

Table 5. Selected Fukui functions of TA, HMTA, BHMTA and DHMTA with higher absolute values at the B3LYP/6-311G (d, p) level of theory.

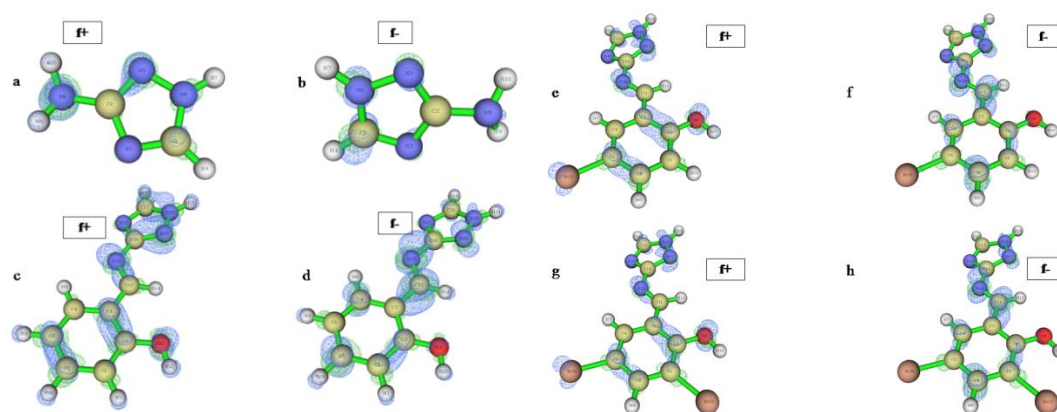
TA			HMTA			BHMTA			DHMTA		
Atom	f^+	f^-	Atom	f^+	f^-	Atom	f^+	f^-	Atom	f^+	f^-
1C	-0.140	-0.267	3C	0.378	-0.219	3C	0.285	-0.255	1C	0.228	-0.238
2C	-0.301	0.378	5C	0.212	-0.010	5C	0.334	-0.125	3C	0.259	-0.268
3N	0.371	-0.374	6C	0.198	-0.336	6C	0.101	-0.262	5C	0.333	-0.138
5N	0.568	-0.436	11O	0.466	-0.369	9O	0.475	-0.366	9O	0.464	-0.344
6N	0.389	-0.405	16C	-0.293	0.294	14C	-0.278	0.304	14C	-0.276	0.311
8N	0.922	-0.446	17N	0.323	-0.320	15N	0.318	-0.319	15N	0.312	-0.318
			19N	0.400	-0.344	17N	0.336	-0.328	17N	0.333	-0.327
			22N	0.530	-0.484	20N	0.433	-0.497	20N	0.418	-0.495
						21Br	0.149	-0.025	21Br	0.132	-0.009
									22Br	0.032	-0.014

In order to confirm the active site of inhibitor binding with the carbon steel surface, the Fukui function (f^+ and f^-) of all the inhibitor molecules is analyzed in Fig. 6. The greater the absolute value of f^+ , the bigger trend to nucleophilic attack and the greater the absolute value of f^- , the bigger trend to nucleophilic attack. The Fukui functions are calculated by Eq. (9) and Eq. (10):

$$f^+ = q_{(N+1)} - q_{(N)} \quad (9)$$

$$f^- = q_{(N)} - q_{(N-1)} \quad (10)$$

where $q_{(N+1)}$, $q_{(N)}$, and $q_{(N-1)}$ are the charges of the atoms in the systems with N+1, N, and N-1 electrons, respectively.

**Figure 6.** Fukui surface distribution of TA (a, b), HMTA (c, d), BHMTA (e, f) and DHMTA (g, h).

It can be seen from Table 5, the nucleophilic attack of TA is more likely occur at the N atoms of amine group and the triazole ring and the electrophilic attack will be more likely occur at the N atom of the triazole ring. The nucleophilic attack of three Schiff bases is more likely occur at the triazole ring, -C-N- groups, benzene ring and the O atom of -OH group. The -C-Br group improves the nucleophilic attack of BHMTA and DHMTA. So introducing the Br atom can improve the reactivity of the Schiff bases, which can enhance the capability for both nucleophilic and electrophilic attacks.

3.5. Dynamic simulations

The molecular dynamics was further used to investigate the interactions between the inhibitors and the Fe(1 1 0) surface. The binding energy between Fe (1 1 0) surface and the Schiff base molecules can be expressed by Eqs(11), (12). [25, 34, 35].

$$E_{\text{adsorption}} = E_{\text{total}} - (E_{\text{surface+solution}} + E_{\text{inhibitor+solution}}) + E_{\text{solution}} \quad (11)$$

$$E_{\text{binding}} = -E_{\text{adsorption}} \quad (12)$$

where E_{total} is the total potential energy of the system, $E_{\text{surface+solution}}$ and $E_{\text{inhibitor+solution}}$ are the potential energies of the system without the SA films and the system without the Fe surface, respectively. E_{solution} is the potential energy of all of the water molecules.

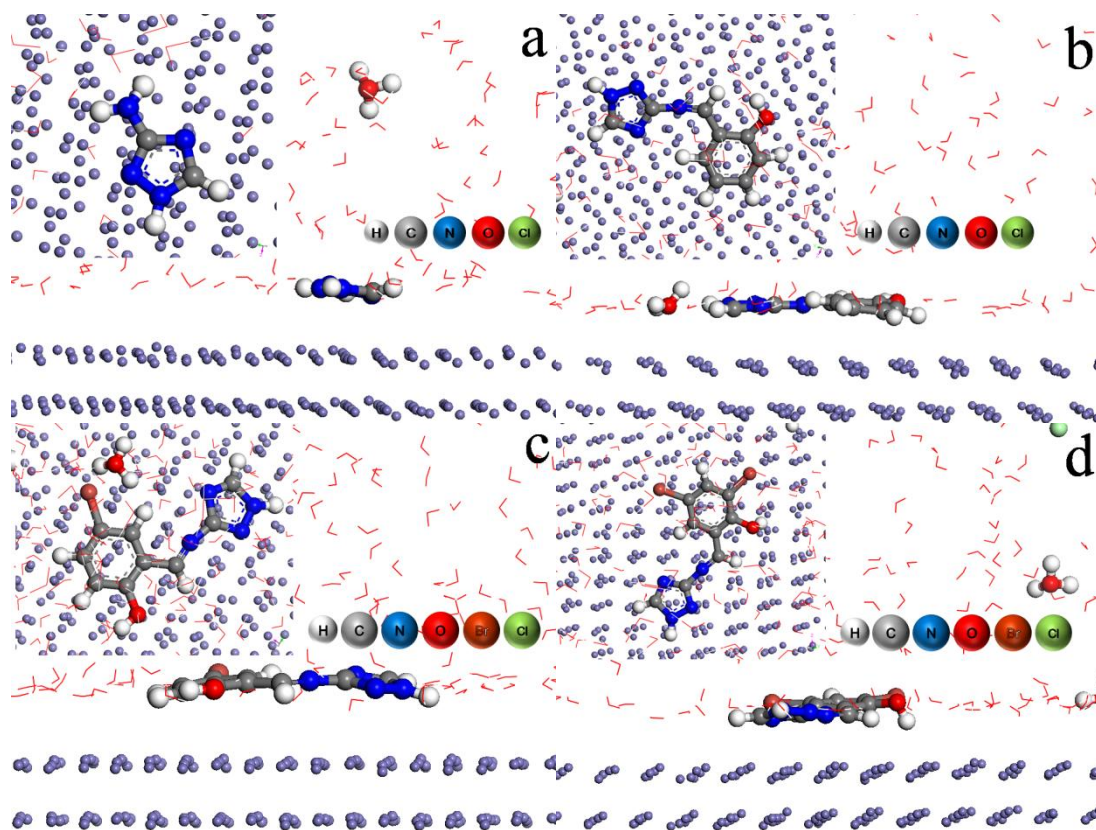


Figure 7. Equilibrium adsorption configuration of inhibitor molecules: TA (a), HMTA (b), BHMTA (c) and DHMTA (d).

The strength of corrosion inhibitors absorbed on the copper surface can be expressed by the binding energy. It can be seen from Fig. 7 all the inhibitor molecules adsorb on the Fe (1 1 0) surface with triazole ring and benzene ring having a planar structure. The $E_{\text{adsorption}}$ and E_{binding} are listed in Table 6. The E_{binding} for the inhibitors follows the order of DHMTA > BHMTA > HMTA > TA, which is consistent with the electrochemical measurements. It can be concluded that the inhibitor compounds form a water-proof films on the iron surface and exhibit high inhibition efficiency which is similar to the conclusions of Ji et al [35].

Table 5. Binding energies and inhibition efficiencies (10 h) of inhibitor molecules.

SA molecules	$E_{\text{adsorption}}$ (eV)	E_{binding} (eV)	$\eta_{10\text{h}}$ (%)
TA	-1.591	1.591	70.43
HMTA	-3.683	3.683	83.83
BHMTA	-3.999	3.999	88.14
DHMTA	-4.044	4.044	92.72

4. CONCLUSION

(1) The investigated SA films of TA, HMTA, BHMTA and DHMTA molecules show excellent performance for inhibition of carbon steel corrosion in 0.5 M HCl.

(2) The inhibition efficiency increases with increasing the self-assembly time in the inhibitor solution concluded from electrochemical measurements. The TA and three Schiff bases act as mixed-type inhibitors for carbon steel in HCl solution.

(3) XPS spectra corroborate the electrochemical measurements and show evidence of the chemisorptions of TA and Schiff bases on the carbon steel surface.

(4) Quantum chemical calculation results reveal that the triazole ring and benzene ring of the Schiff base molecules are the active sites by which the inhibitor can adsorb onto the carbon steel surface by sharing of electrons with iron atoms.

(5) Molecular dynamics simulation results reveal that all the inhibitors adsorb on the iron surface in a nearby flat manner.

ACKNOWLEDGEMENTS

This work was funded by the Guangxi Nature Science Foundation (No. 2016GXNSFJJA120133) and the key project of science and technology research in universities of Guangxi (2013ZD029).

References

1. M. V. Karavaeva, S. K. Liseleva, A. V. Ganeev, E. O. Protasova, M. M. Ganiev, L. A. Simonova, R. Z. Valiev, *J. Meter. Sci.*, 50 (2015) 6730.

2. Y. Mine, K. Hirashita, H. Takashima, M. Matsuda, K. Takashima, *Mater. Sci. Eng. A*, 560 (2013) 535.
3. M. Gopiraman, P. Sakunthala, D. Kesavan, V. Alexramani, I. S. Kim, N. Sulochana, *J. Coat. Technol. Res.*, 9 (2012) 15.
4. A. Ulman, *Chem. Rev.*, 96 (1996) 1533.
5. W. Liu, W. Cao, X. Deng, Y. Min, Q. Xu, *Int. J. Electrochem. Sci.*, 10 (2015) 8858.
6. F. Yu, S. Chen, H. Li, L. Yang, Y. Yin, *Thin solid films*, 520 (2012) 4990.
7. K. C. R. Ferreira, R. F. B. Cordeiro, J. C. Nunes, H. Orofino, M. Magalhães, A. G. Torres, E. D'Elia, *Int. J. Electrochem. Sci.*, 11 (2016) 406.
8. V.V. Torres, V.A. Rayol, M. Magalhães, C.M. Viana, L.C.S. Aguiar, S.P. Machado, H. Orofino, E. D'Elia, *Corros. Sci.*, 79 (2014) 108.
9. K. Shalabi, Y.M. Abdallah, Hala M. Hassan, A.S. Fouda, *Int. J. Electrochem. Sci.*, 9 (2014) 1468.
10. K.M. Zohdy, *Int. J. Electrochem. Sci.*, 10 (2015) 414.
11. A. O. W. Neto, E. F. Moura, H. S. Júnior, T. N. C. Dantas, A. A. D. Neto, A. Gurgel, *Colloid. Surface. A.*, 398 (2012) 76.
12. E. C. Roberto, A. O. W. Neto, C. A. Martínez-Huitle, J. L. C. Fonseca, T. N. C. Dantas, A. Gurgel, *Prog. Org. Coat.*, 76 (2013) 1308.
13. M. A. Hegazy, A. M. Hasan, M. M. Emar, M. F. Bakr, A. H. Youssef, *Corros. Sci.*, 65(2012) 67.
14. N. Soltani, H. Salavati, N. Rasouli, M. Pazireh, A. Moghadasi, *Chem. Eng. Commun.*, 203 (2016) 840.
15. N. A. Negm, F. M. Ghuiba, S. M. Tawfik, *Corros. Sci.*, 53 (2011) 3566.
16. K. R. Ansari, M. A. Quraishi, A. Singh, *Corros. Sci.*, 79 (2014) 5.
17. K. M. Khan, S. Siddiqui, M. Saleem, M. Taha, S. M. Saad, S. Perveen, M. I. Choudhary, *Bioorgan Med. Chem.*, 22 (2014) 6509.
18. Y. M. Issa, H. B. Hassib, H. E. Abdelaal, *SpectrochimActa A.*, 74 (2009) 902.
19. Z H Chohan, M H Anif, *Appl. Organomet. Chem.*, 25 (2011) 753.
20. M. J. Frisch, G. W. Trucks, H. B. Schlegel, G. E. Scuseria, M. A. Robb, J. R. Cheeseman, J. A. Montgomery, Jr., T. Vreven, K. N. Kudin, J. C. Burant, J. M. Millam, S. S. Iyengar, J. Tomasi, V. Barone, B. Mennucci, M. Cossi, G. Scalmani, N. Rega, G. A. Petersson, H. Nakatsuji, M. Hada, M. Ehara, K. Toyota, R. Fukuda, J. Hasegawa, M. Ishida, T. Nakajima, Y. Honda, O. Kitao, H. Nakai, M. Klene, X. Li, J. E. Knox, H. P. Hratchian, J. B. Cross, C. Adamo, J. Jaramillo, R. Gomperts, R. E. Stratmann, O. Yazyev, A. J. Austin, R. Cammi, C. Pomelli, J. W. Ochterski, P. Y. Ayala, K. Morokuma, G. A. Voth, P. Salvador, J. J. Dannenberg, V. G. Zakrzewski, S. Dapprich, A. D. Daniels, M. C. Strain, O. Farkas, D. K. Malick, A. D. Rabuck, K. Raghavachari, J. B. Foresman, J. V. Ortiz, Q. Cui, A. G. Baboul, S. Clifford, J. Cioslowski, B. B. Stefanov, G. Liu, A. Liashenko, P. Piskorz, I. Komaromi, R. L. Martin, D. J. Fox, T. Keith, M. A. Al-Laham, C. Y. Peng, A. Nanayakkara, M. Challacombe, P. M. W. Gill, B. Johnson, W. Chen, M. W. Wong, C. Gonzalez and J. A. Pople, Gaussian, Inc., Wallingford, CT, 2004.
21. G. Gece, S. Bilgiç, *Corros. Sci.*, 52 (2010) 3435.
22. Materials Studio, Revision 6.0, Accelrys Inc., San Diego, USA, 2011.
23. L. Guo, S. T. Zhang, T. M. Lv, W. J. Feng, *Res. Chem. Intermed.*, 41 (2015), 3729.
24. B. Hirschorn, M. E. Orazem, B. Tribollet, V. Vivier, I. Frateur, M. Musiani, *Electrochim. Acta.*, 55 (2010) 6218.
25. Z. Zhang, N. Tian, X. Li, L. Zhang, L. Wu, Y. Huang, *Appl. Surf. Sci.*, 357 (2015) 845.
26. H. Liu, L. Zhu, Q. Zhao, *Res Chem Intermed*, 41 (2015) 4943.
27. Z. Zhang, N. Tian, L. Zhang, L. Wu, *Corros. Sci.*, 98 (2015) 438.
28. I. Ahmad, R. Prasad, M. A. Quraishi, *Corros. Sci.*, 52 (2010) 3033.
29. A. S. Fouda, M. Abdallah, M. Medhat, *Physicochemical problems of materials protection*, 48 (2012) 477.
30. Available: <http://www.lasurface.com/database/elementxps.php> (18/12/2014).

31. H. Zhao, X. Zhang, L. Ji, H. Hu, Q. Li, *Corros. Sci.*, 83 (2014) 261.
32. F. Zhang, Y. Tang, Z. Cao, W. Jing, Z. Wu and Y. Chen, *Corros. Sci.*, 61 (2012)1.
33. I. Lukovits, E. Lalman, F. Zucchi, *Corrosion*, 57 (2001)3.
34. S. K. Saha, P. Ghosh, A. Hens, N.C. Murmu, P. Banerjee, *Physica E: Low-dimensional systems and nanostructures*, 66 (2015) 332.
35. Y. Ji, B. Xu, W. Gong, X. Zhang, X. Jin, W. Ning, Y. Meng, W. Yang, Y. Chen, *Journal of Taiwan institute of chemical engineers*, 66 (2016) 301.

© 2017 The Authors. Published by ESG (www.electrochemsci.org). This article is an open access article distributed under the terms and conditions of the Creative Commons Attribution license (<http://creativecommons.org/licenses/by/4.0/>).